RVE model development for bending analysis of three-core submarine power cables with dashpot-enhanced periodic boundary conditions

Li, Xiao; Liu, Zhuangjian; Jiang, Xiaoli; Hopman, Hans

DOI
10.1016/j.oceaneng.2024.118588

Publication date
2024

Document Version
Final published version

Published in
Ocean Engineering

Citation (APA)
Li, X., Liu, Z., Jiang, X., & Hopman, H. (2024). RVE model development for bending analysis of three-core submarine power cables with dashpot-enhanced periodic boundary conditions. *Ocean Engineering*, *309*, Article 118588. https://doi.org/10.1016/j.oceaneng.2024.118588

Ocean Engineering 309 (2024) 118588

Contents lists available at ScienceDirect

Ocean Engineering

journal homepage: www.elsevier.com/locate/oceaneng

Research paper

RVE model development for bending analysis of three-core submarine power cables with dashpot-enhanced periodic boundary conditions

Xiao Li [a,*], Zhuangjian Liu [a], Xiaoli Jiang [b], Hans Hopman [b]

[a] Institute of High Performance Computing (IHPC), Agency for Science, Technology and Research (A*STAR), 1 Fusionopolis Way, #16-16 Connexis, Singapore 138632, Republic of Singapore

[b] Department of Maritime and Transport Technology, Delft University of Technology, Netherlands

ARTICLE INFO

Keywords:
Submarine power cable
Bending stiffness
Representative Volume Element (RVE)
Thermal effect
Finite element method (FEA)

ABSTRACT

Submarine power cables in offshore wind farm operate within a complex multiphysics environment. Despite being designed to be both flexible and robust though, their mechanical characteristics are susceptible to variations of thermal field. Bending studies of submarine power cables present challenges rooted in geometry complexity, component contact, and material non-linearity, compounded by the intricate stick–slip mechanism. The difficulty is further intensified when incorporating the thermal impact on material and contact properties. This paper presents a three-dimensional Representative Volume Element (RVE) model for predicting the nonlinear bending stiffness of three-core submarine power cables. The RVE model, developed with constant curvature and periodic boundary conditions, incorporates dashpots to address the stick–slip challenges associated with cable bending. This modeling approach minimizes the required cable length for bending analysis, significantly reducing computational costs. Validation against the bending test of a three-core cable at room temperature, alongside comparison with a 3D full-scale finite element (FE) model, demonstrates the efficiency and accuracy of the proposed RVE approach. Furthermore, the study explores the thermal effect on cable bending, highlighting the capabilities of the proposed RVE model in facilitating thermal–mechanical coupled flexural analysis of submarine power cables. This research contributes to advancing understanding and optimization of submarine power cable design for offshore applications.

1. Introduction

The expansion of offshore wind farms is rapidly accelerated by the growing demand for renewable energy nowadays. Submarine power cables, as one key component of offshore wind systems, have to meet stringent requirements to efficiently transport electricity and endure the environmental conditions (DeCastro et al., 2019). Unlike most offshore energy infrastructure, submarine cables operate within complex physical environments where mechanical, thermal and electromagnetic fields interact simultaneously (Matine and Drissi-Habti, 2019; Wang et al., 2021). Understanding their mechanical performance while taking into account the influence of correlated physical fields can help optimize cable designs, identify potential risks, and prevent premature failures (Yan et al., 2021, 2022).

Bending stiffness stands out as a crucial mechanical property in design phase, allowing cables to withstand substantial wave-induced motion without suffering internal damage (Hall et al., 2021). Nonetheless, the public literature currently lacks comprehensive cable bending studies, primarily due to the intricate nature of cable geometry and contact mechanisms. Functional elements like armor wires and conductors are helically arranged within the body, imparting compliance to the submarine cable, as shown in Fig. 1(COREWIND, 2020). The penalty is, however, the assessment of bending stiffness becomes difficult due to the stick–slip behaviors of those helix elements (Skeie et al., 2012).

The cross-sectional configuration of a typical three-core submarine power cable is illustrated in Fig. 2. The cable comprises several main components arranged from the outermost to the innermost, including: an outer sheath to safeguard the cable from external mechanical damage; armors for mechanical protection which are wound helically; an inner liner shielding the underlying components from physical damage like abrasion and impact; steel strands providing additional mechanical protection and weight support, contributing to a round cross-section in conjunction with cores and fillers; an insulation system to prevent electricity leakage, and conductors for power transmission (Resner and Paszkiewicz, 2021).

Companies like Nexans and Prysmian (Maioli, 2015; Komperød et al., 2017) have conducted experiments to investigate the bending behavior of submarine power cables. Their tests revealed that the bending

* Corresponding author.
E-mail address: li_xiao@ihpc.a-star.edu.sg (X. Li).

https://doi.org/10.1016/j.oceaneng.2024.118588
Received 25 April 2024; Received in revised form 6 June 2024; Accepted 23 June 2024
Available online 1 July 2024

Nomenclature

Abbreviations

DoF	degree of freedom
FE	finite element
MPC	multiple point constraint
RVE	representative volume element

Symbols

α	laying angle
ρ	bending radius
σ_u	ultimate tensile strength
σ_y	yield strength
θ	angular parameter
φ	bending angle
$\{\Gamma\}$	cross section
A, B, C, O, S	points
c_d	dashpot coefficient
D_0, D_1, D_2	constants
E	elastic modulus
K	temperature
L_p	pitch of armor layer
L_R	cable length in RVE
l_w	pitch of helical wire
M	bending moment
N	natural number
n	wire number
q	Euler parameter
R	element of rotation matrix
U	matrix element
x, u	initial coordinate and displacement, respectively
$\boldsymbol{\Delta}$	partial derivatives
$\mathbf{e}-\boldsymbol{\Phi}$	axis-angle representation
$\mathbf{f}$	constraint equation
$\mathbf{I}$	identity matrix
$\mathbf{Q}$	unit quaternion
$\mathbf{R}$	rotation matrix
$\mathbf{t}-\mathbf{n}-\mathbf{b}$	Frenet–Serret frame
$\mathbf{x}, \mathbf{u}$	initial position and displacement vector, respectively
$\hat{t}, \hat{n}, \hat{b}$	Tait-Bryan angle
X − Y − Z	universe Cartesian coordinate system

Subscripts

i, j, k	index
r	point position after rotation

stiffness of submarine cables is highly nonlinear, varying with bending curvature (Jordal et al., 2017; Tyrberg et al., 2019). Submarine cables exhibit hysteresis in their flexural response, attributed to the stick–slip mechanism among the components. Under small curvature, internal friction prevents slip, resulting in a high initial tangent stiffness. As the curvature increases to a critical value, friction is overcome, leading to slippage and a subsequent reduction in stiffness (Sævik and Ye, 2016; Kebadze, 2000; Kraincanic and Kebadze, 2001).

Moreover, tests conducted by these companies indicate that the bending stiffness of submarine cables is sensitive to thermal variations (Maioli, 2015; Komperød et al., 2017). In cases where cables

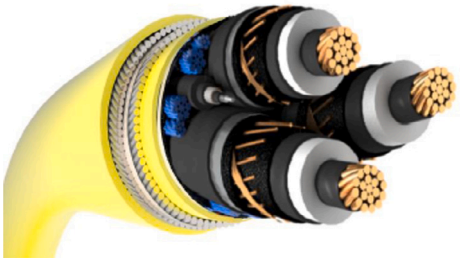

Fig. 1. Helical configuration of a typical three-core submarine power cable (COREWIND, 2020).

transmit high electric current, the energy loss in the conductor induces resistive heating, warming both the cable body and the surrounding environment. This operational condition may result in volume expansion and mechanical degradation of components, thereby influencing the bending performance of submarine power cables (Hamdan, 2019). The complexity of the flexural response is further compounded when considering the viscosity of the anti-corrosion bitumen (Mullins et al., 2015; Hedlund, 2015).

To improve the flexural design, mathematical modeling is essential to help understand the bending characteristics. Analytical models for cable bending stiffness can establish upper and lower bounds by assuming either full slip or full stick conditions among the helical components (Lanteigne, 1986; Kraincanic and Kebadze, 2001; Ramos et al., 2003). The full slip condition assumes that all helices slip during bending and sums up the bending stiffness values of individual components. Conversely, the stick condition assumes that all the cable components are fully bonded, calculating the bending stiffness by treating the cable as an integral, solid structure.

Recent advances in analytical modeling concentrate on addressing the slippage behaviors of helical armor layers, given their hysteresis effect in bending (Zhang et al., 2023b; Tang et al., 2022; Yun et al., 2020). By assuming a prescribed slippage route for the armor wires, their bending stiffness is calculated using Kirchhoff's rod theory (Kirchhoff, 1859; Sævik, 2011; Li et al., 2019). Mostly, two route assumptions – loxodromic and geodesic hypotheses – define the slippage route of helices in bending. The loxodromic hypothesis assumes a constant laying angle during helical wire deformation, resulting in a loxodromic curve on a torus surface (Witz and Tan, 1992; Skeie et al., 2012). In geodesic hypothesis, the helical wire is assumed to take the path yielding the shortest distance on the torus surface, following the principle of minimum potential energy (Feret and Bournazel, 1987; Out and Morgen, 1997; Leroy and Estrier, 2001).

The development of current analytical models is still impeded by incorporating factors such as initial states and component interactions (Li et al., 2021a; Ménard and Cartraud, 2021, 2023). As a result, numerical analysis has become the predominant approach in the studies of cable bending. Constructing three-dimensional finite element (FE) models with geometry details allows better insight into the structural integrity and layer interactions (Chang and Chen, 2019; Guttner et al., 2017). However, it poses computational challenges due to the incorporation of helical structural elements and multiple contact regions (Li et al., 2021b; Fang et al., 2023), let alone the introduction of thermal effects. Overall, 3D FE simulations of submarine power cables are still confined to analyzing responses under axisymmetric loading such as tension or torsion (Chang and Chen, 2019; Yan et al., 2022; Yang et al., 2021; Lu et al., 2017a).

To reduce the computational cost, simplified FE models are developed as an alternative strategy. One common simplification is replacing the solid helical metal strands or wires with beam or shell elements (Corre and Probyn, 2009; Lu et al., 2017b). While this approach enables the mechanical analysis of cables under complex loading conditions, it raises concerns regarding element equivalence and layer

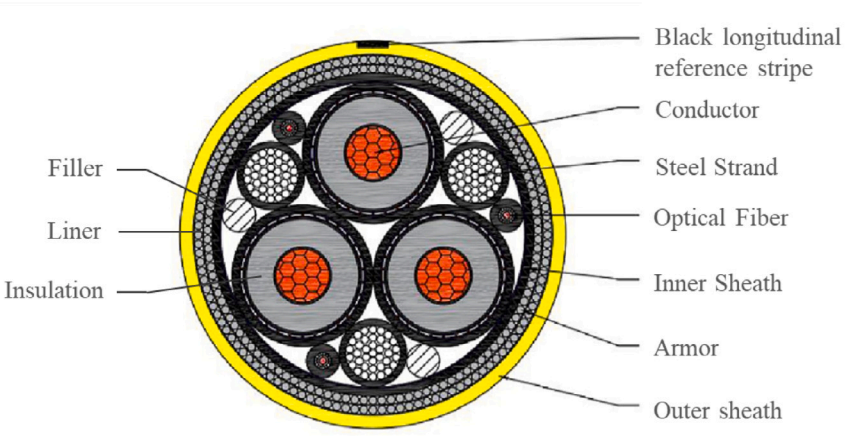

Fig. 2. Typical cross section of a three-core submarine power cable.

contact as the involvement of beam and shell elements (Ménard and Cartraud, 2021, 2023). Furthermore, this simplification also requires the model to be built with adequate length in order to eliminate end effects (Axelsson and Skjerve, 2014).

Another simplification is to reduce the cable length using a Representative Volume Element (RVE) model with periodic boundary conditions (Lukassen et al., 2019; Tjahjanto et al., 2017). In this approach, one cable portion called "unit cell" is "cut off" to represent the "infinitely long" submarine cable line. With the aid of displacement couplings and kinematic constrains at the cutting ends, the entire bent cable could be represented by such a unit cell. While this RVE modeling technique offers computational efficiency in cables' bending analysis, the model quality heavily relies on the adopted periodic boundary conditions (Li et al., 2021b; Smith et al., 2023). Determining suitable periodic boundary conditions to accurately reflect the stick–slip characteristics of submarine power cables faces significant challenges in RVE model development.

Currently, there are few available models that effectively balance accuracy and efficiency for cable bending analysis. Furthermore, there is a continuous demand for integrating thermal effects into cable bending studies, as supported by tests demonstrating the significant temperature sensitivity of cable bending stiffness (Tyrberg et al., 2019; Komperød et al., 2017). In respond to this, an RVE model, with dashpot-enhanced periodic boundary conditions, is presented.

The rest of the paper is organized as follows: in Section 2, the methodology is outlined for developing an RVE model of a three-core submarine power cable. Section 3 presents the mechanical test on a three-core submarine cable sample, and the result is employed in Section 4 for model validation. Moreover, a 3D full-scale FE model is constructed in Section 4, and its result is compared with the RVE model for computational efficiency assessment. Section 5 investigates the thermal effect on bending stiffness of cables using this validated RVE model and discussions are given. The conclusions are presented in the final section.

2. RVE technique and model development

The RVE is a 3D-periodic model that assumes the bent cable experiences constant curvatures over time (Caleyron et al., 2014). With this assumption, all helical wires within a specific armor layer can be treated to have the same behavior, making it feasible to apply periodic boundary conditions onto a representative cable cell. This section begins with a mathematical description of the periodic boundary conditions for helices in bent cables, followed by the subsequent implementation of RVE in the commercially available finite element code ABAQUS (Simulia, 2022).

2.1. Periodicity of helices under bending

Considering a straight cylinder helically wound by wires with a laying angle α, as illustrated in Fig. 3. Under the assumption of constant curvature, a periodic repetition of behaviors occurs for points on the wires at the same angular position on the cross-section. This periodicity is exemplified by points A and B in Fig. 3, both marked with an angular parameter θ. A universe Cartesian coordinate system X-Y-Z is established as shown in this figure to which everything discussed can be referenced. The Frenet–Serret frame, denoted as **t**-**n**-**b**, is established on the center-line of the cylinder within its tubular domain, represented by the intersection cross-sections labeled as $\{\Gamma\}$. The cross-sections corresponding to points A and B are labeled as $\{\Gamma(0)\}$ and $\{\Gamma(1)\}$, with their origins situated at points O and C, respectively.

When the cylinder is subjected to a bending moment M, the motions of attached wires follow the loxodromic paths in the absence of slippage. Correspondingly, the cross-section $\{\Gamma(1)\}$ is rotated to a new location $\{\Gamma(1)\}_r$ with the bending angle φ. The point B, belonging to one of the wires within $\{\Gamma(1)\}$, is also repositioned to a new position B_r. In the event that slippage occurs, the wire will slide over the external surface of the cylinder in search of a natural path, leading the attached point to position B_1. Consequently, the displacement vector from point B to B_1 is given as:

$$\overrightarrow{BB_1} = \overrightarrow{BB_r} + \overrightarrow{B_rB_1} \tag{1}$$

Noting that:

$$\begin{cases} \overrightarrow{BB_r} = \overrightarrow{C_1B_r} - \overrightarrow{CB} = \mathbf{R}\overrightarrow{CB} - \overrightarrow{CB} \\ \overrightarrow{B_rB_1} = \mathbf{R}\overrightarrow{AA_1} \end{cases} \tag{2}$$

we have:

$$\overrightarrow{C_1B_1} = \mathbf{R}(\overrightarrow{CB} + \overrightarrow{AA_1}) \tag{3}$$

where $\mathbf{R}$ is a rotation matrix that describes the relationship of one coordinate system relative to another, taking a general form as:

$$\mathbf{R} = \begin{bmatrix} R_{11} & R_{12} & R_{13} \\ R_{21} & R_{22} & R_{23} \\ R_{31} & R_{32} & R_{33} \end{bmatrix} \tag{4}$$

Here, R denotes the matrix element. The cylinder with helical wires attached is not a fully axisymmetric structure. In other words, frame $\{\Gamma(1)\}$ undergoes a twist during bending. According to Euler's rotation theorem (Euler), any 3D rotation (or sequence of rotations) can be specified using two parameters: a unit vector $\mathbf{e}$ that defines an axis of rotation; and an angle Φ describes the magnitude of the rotation about that axis, as illustrated in Fig. 4. Therefore, a pseudo-vector $\mathbf{\Phi}^C$ is employed to describe the rotation $\mathbf{R}(\mathbf{\Phi}^C)$ of frame $\{\Gamma(1)\}$ about point C.

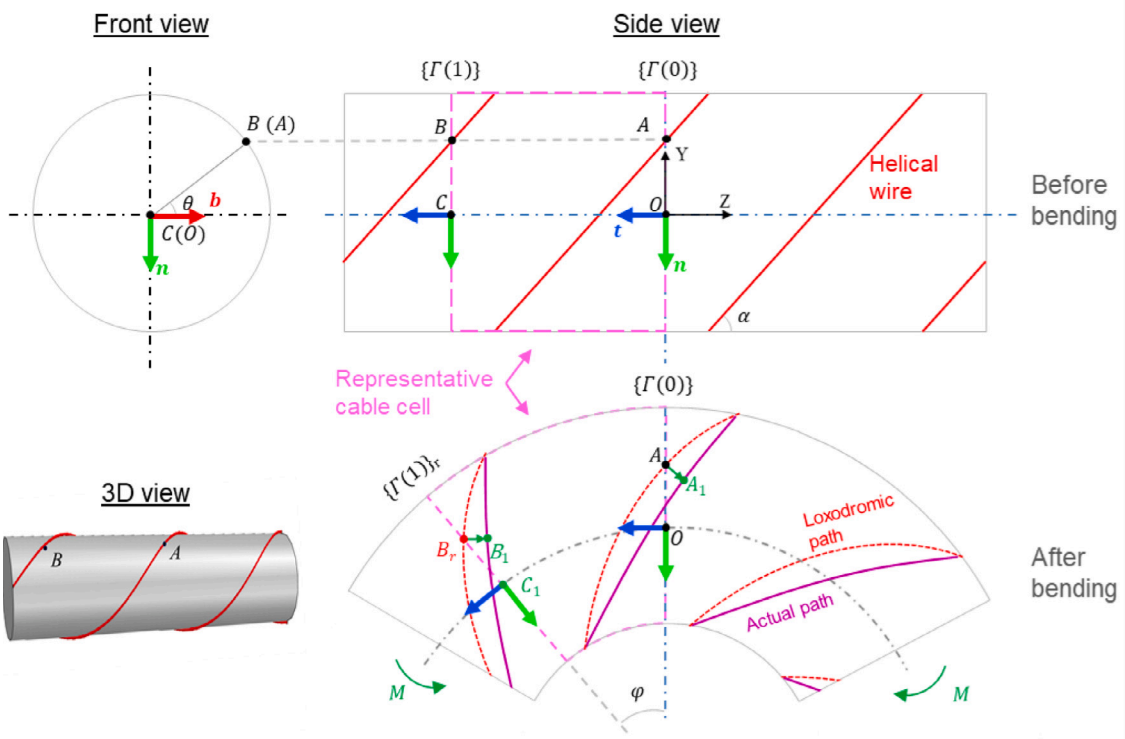

Fig. 3. Kinematics periodicity of helical wire in cables: pre- and post-bending.

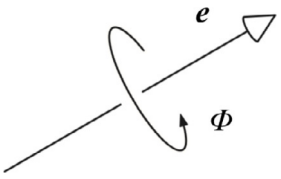

Fig. 4. Axis-angle representation.

This axis-angle representation can be expressed by a 4 × 1 vector called unit quaternion as:

$$\mathbf{Q} = [q_0 \ q_1 \ q_2 \ q_3]^T \tag{5}$$

where:

$$\begin{bmatrix} q_0 \\ q_1 \\ q_2 \\ q_3 \end{bmatrix} = \begin{bmatrix} \cos(\hat{n}/2) \\ 0 \\ 0 \\ \sin(\hat{n}/2) \end{bmatrix} \begin{bmatrix} \cos(\hat{b}/2) \\ 0 \\ \sin(\hat{b}/2) \\ 0 \end{bmatrix}^T \begin{bmatrix} \cos(\hat{t}/2) \\ \sin(\hat{t}/2) \\ 0 \\ 0 \end{bmatrix} \tag{6}$$

Here, $\hat{n}$, $\hat{b}$, and $\hat{t}$ represent Tait–Bryan angles with respect to their corresponding axes. It is clear that the four Euler parameters are not independent:

$$q_0^2 + q_1^2 + q_2^2 + q_3^2 = 1 \tag{7}$$

The rotation matrix $\mathbf{R}(\mathbf{\Phi}^C)$ that is equivalent to a set of Euler parameters is:

$$\mathbf{R}(\mathbf{\Phi}^C) = \begin{bmatrix} 1-2q_2^2-2q_3^2 & 2(q_1q_2-q_3q_0) & 2(q_1q_3+q_2q_0) \\ 2(q_1q_2+q_3q_0) & 1-2q_1^2-2q_3^2 & 2(q_2q_3-q_1q_0) \\ 2(q_1q_3-q_2q_0) & 2(q_2q_3+q_1q_0) & 1-2q_1^2-2q_2^2 \end{bmatrix} \tag{8}$$

Denoting $\mathbf{x}^{(\cdot)}$ and $\mathbf{u}^{(\cdot)}$ as the initial position and displacement vector of the corresponding points $(\cdot)$, Eq. (3) can rewritten into a constraint equation as:

$$\mathbf{f} = \mathbf{u}^B - \mathbf{R}(\mathbf{x}^B - \mathbf{x}^C + \mathbf{u}^A) - \mathbf{u}^C - \mathbf{x}^C + \mathbf{x}^B = 0 \tag{9}$$

Implementing this constraint equation in Abaqus using Multiple Point Constraint (MPC) user-subroutine enables the realization of periodic behaviors for helical components in RVE.

2.2. RVE modeling

2.2.1. Constraint for constant curvature

The bending behavior of the armor layer, consisting of n wires, repeats at a regular pitch-length interval as:

$$L_p = \frac{l_w}{n} \tag{10}$$

where l_w is the pitch of helical wires in armor layer. To ensure periodic conditions in the RVE modeling, the model length L_R should be a multiple of the layer pitch, given by $L_R = N \cdot L_p$, where N is a natural number. For arbitrary point S_i lies on the center-line between point C and O, as shown in Fig. 5, its degrees of freedom (DoFs) shall meet the following constraint equations due to the constant curvature assumption:

$$\begin{cases} f_2^{S_i} = u_2^{S_i} - \rho(1-\cos u_4^{S_i}) = 0 \\ f_3^{S_i} = u_3^{S_i} - \rho \sin u_4^{S_i} + x_3^{S_i} = 0 \end{cases} \tag{11}$$

in which:

$$u_4^{S_i} = u_4^C \frac{x_3^{S_i}}{x_3^C} \tag{12}$$

And the bending radius ρ is calculated as:

$$\rho = \frac{x_3^C + u_3^C}{\sin u_4^C} \tag{13}$$

Here, $f_j^{S_i}$ denotes the constraint equation for point S_i in its j-th DoF; x_j represents the initial coordinate, and u_j represents the DoFs in the universal Cartesian coordinate system X-Y-Z; the subscript 'j' ranges from 1 to 3 for displacement along the X, Y, and Z axes, and from 4 to 6 for corresponding rotational quantities. The constraint equation set Eqs. is embedded into Abaqus MPC user subroutine, enforcing a constant

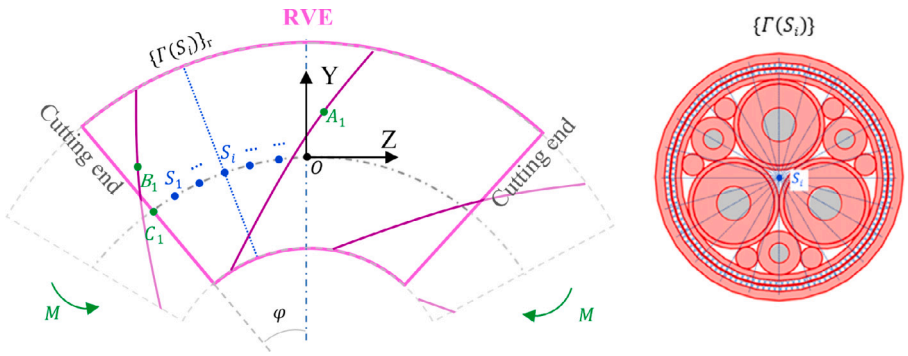

Fig. 5. Constant curvature for the center-line of RVE.

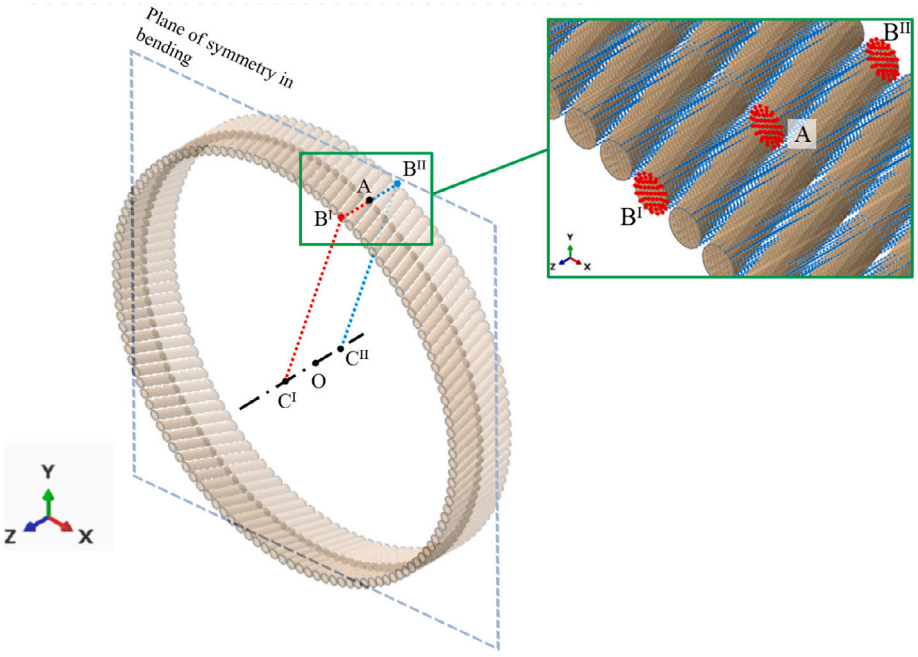

Fig. 6. Implementation of periodic boundary condition in RVE.

curvature along the centerline of the cable. Each point S_i on this line controls its respective cross-section $\Gamma(S_i)$ using kinematic coupling, as shown in Fig. 5, ensuring uniform bending across the entire RVE. In what follows, the applied boundary conditions at the cutting ends of the RVE are given in details.

2.2.2. Constraints on cutting ends

In our model, the RVE is designed with a length of $2L_p$ to create a symmetry bending plane in the middle, as illustrated in Fig. 6. As a result, the node groups of the wires on the cutting ends, denoted as {B}, are governed by both the node group {A} on middle section and the point C to achieve periodicity. The governing equation, Eq. (9), is implemented as an MPC-type constraint using the user subroutine in Abaqus. Due to the incremental nature of the solution procedure in Abaqus/Standard, this governing equation is linearized into a set of constraints as:

$$\mathrm{d}\mathbf{f} = \mathrm{d}\mathbf{u}^B - \mathrm{d}\mathbf{R}(\mathbf{x}^B - \mathbf{x}^C + \mathbf{u}^A) - \mathbf{R}\mathrm{d}\mathbf{u}^A - \mathrm{d}\mathbf{u}^C = 0 \tag{14}$$

The partial derivatives $\boldsymbol{\Delta}$ of the constraint equation $\mathbf{f}$ with respect to each nodal degree of freedom for node groups {A}, {B}, and point C can be expressed in arrays as follows:

$$\begin{aligned}
\boldsymbol{\Delta}^A &= \frac{\partial \mathbf{f}}{\partial \mathbf{u}^A} = -\mathbf{R} \\
\boldsymbol{\Delta}^B &= \frac{\partial \mathbf{f}}{\partial \mathbf{u}^B} = \mathbf{I} \\
\boldsymbol{\Delta}^C &= \frac{\partial \mathbf{f}}{\partial \mathbf{u}^C} = \begin{bmatrix} -1 & 0 & 0 & U^C_{41} & U^C_{51} & U^C_{61} \\ 0 & -1 & 0 & U^C_{42} & U^C_{52} & U^C_{62} \\ 0 & 0 & -1 & U^C_{43} & U^C_{53} & U^C_{63} \end{bmatrix}
\end{aligned} \tag{15}$$

where:

$$U^C_{kj} = \frac{\partial R_{j(k-3)}}{\partial u^C_k}(x^B_j - x^C_j + u^A_j) \tag{16}$$

Here, $\mathbf{I}$ is the identity matrix; the subscript 'k' ranges from 4 to 6, representing rotational quantities about the X, Y, and Z axes, respectively. Simultaneously, the subscript 'j' ranges from 1 to 3 with the same definition as mentioned above.

In addition to the periodic boundary condition of wires, constraints are also applied to the cutting ends of remaining components. Kinematic couplings are employed to constrain the nodes of all non-metallic components at the cutting ends, in which their six DoFs are governed by the corresponding point C. Metallic components within the core region

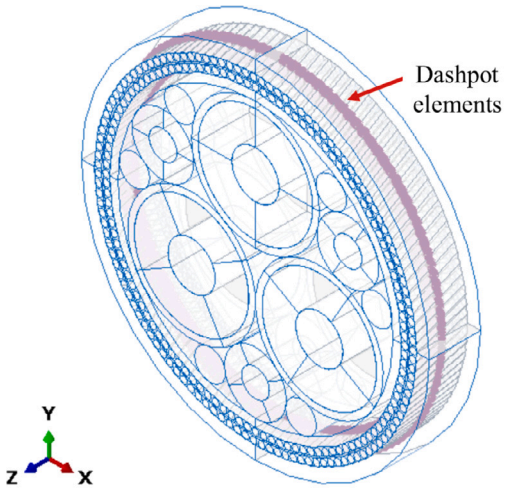

Fig. 7. Dashpot elements connect to node group {A} on wires.

are unrestricted at their cutting ends, allowing relative movement between them and their adjacent polymeric layers. Except for the helical wires, nodes of all components on the middle plane are fully fixed, enabling the symmetrical bending. Ultimately, with these constraints in place, the bending moments applied to governing points C^{I} and C^{II} are effectively transferred to the RVE.

2.2.3. Interactions between components

Simulating cable bending through RVEs poses challenges, especially in addressing the interaction between components. Helical wires, wrapping around the cable core, may exhibit stick–slip behaviors during bending. In practical cable bending scenarios, the loads acting on helical wires are transferred through contact interfaces with neighboring components. The critical factor determining whether the wire slip or not is the balance between its shear force and friction (Kebadze, 2000).

In RVEs, the bending of the cable is controlled by a designated point, referred to as point C, at each end. This point also serves as a governing factor for establishing the periodic boundary conditions of the helical wires. It is important to note that in RVEs, the helical wires are correspondingly shortened into segments. Due to the misalignment between the helical axis and the cable centerline, the helical wire "segments" in RVEs are compelled to experience both torsional deformation and rotational movement according to the traction from point C. Consequently, the periodic constraints in RVEs cause the helical armor wires to have reduced adherence compared to their counterparts in cables subjected to real-world bending conditions.

To resolve this, a dashpot technique is introduced, utilizing dashpot elements to counteract the traction effect from point C, as illustrated in Fig. 7. These elements are connected to the node group {A} of wires at the middle plane, associating with their degree of freedom u_3 and featuring a damping coefficient c_d. This adds a "velocity"-dependent damping force to the connected node group, where velocity is the ratio of displacement increment to analytical time increment in Abaqus static analysis (Simulia, 2022). Essentially, these dashpots dampen the sudden slippage caused by the traction from point C, leaving the stick–slip to be determined solely by the balance between shear force and friction. Calibration for the damping coefficient c_d of the dashpot elements is provided in the following sections.

Component contact arises during the loading process as the submarine power cable is a multi-layered tubular structure. To address this, a surface-based penalty method is employed. According to the work of Kinsella, et al. (2005) and Gay Neto and Martins (2014) (Kinsella et al., 2005; Gay Neto and Martins, 2014), a Coulomb friction coefficient of 0.25 is adopted for the tangent sliding between layers while a penalty stiffness factor of 0.1 is used in normal contact. An 8-node coupled temperature–displacement element, C3D8RT, is employed in RVE to enable the mechanical, thermal and their coupling analysis. By using the sweep meshing technique, the RVE is meshed as shown in Fig. 8.

Bending moments are symmetrically applied to reference points C^{I} and C^{II}. The boundary condition for both C^{I} and C^{II} permits movement exclusively in the y-z plane. Simultaneously, point O located in the middle bending plane is fully fixed. By encoding the aforementioned constraint equations into Fortran user subroutine, the RVE model for coupled mechanical–thermal analysis of submarine power cables is thereby developed.

3. Bending tests of submarine cable

This section presents the bending tests carried out on three-core submarine power cable. The bending stiffness data obtained from this test are utilized for model validation in subsequent sections. Before the bending test, measurements of the mechanical performance were undertaken specifically on polymers used for insulation and protection sheaths. Due to confidentiality concerns, not all test data are presented, and the disclosed data are normalized.

3.1. Tests for material properties

The three-core cable sample provided by the manufacturer is designed to operate within a core temperature range of 80 to 100 °C. The primary materials used in cable fabrication include: copper for the conductors; steels for armor wires and strands; XLPE for insulation; MDPE for fillers, liner and inner sheath; and HDPE for the outer sheath. Metallic materials are assumed to maintain their mechanical properties unchanged regardless of thermal variations. However, for polymeric materials, given that their mechanical properties are influenced by the manufacturing process and undergo significant changes with temperature, material tests are conducted by cutting samples from the tested cable. Fig. 9 displays the test samples for MDPE, HDPE, and XLPE along with the property measurement.

The mechanical properties of the tested polymers are presented in Fig. 10. Notably, only XLPE samples undergo testing for varying thermal conditions, as they are used in insulation system to cover the innermost conductors. Material tests for MDPE and HDPE are conducted at 20 °C though, their mechanical properties at various temperatures can be derived through equation fitting as below (Amjadi and Fatemi, 2020):

$$\sigma_y,\ \sigma_u,\ E = D_0 + D_1 \cdot K + D_2 \cdot K^2 \tag{17}$$

where σ_y, σ_u, and E are yield strength, ultimate tensile strength, and elastic modulus, respectively; D_0, D_1, and D_2 are constants to be fitted; K is the temperature.

3.2. Bending test on submarine cable

The bending stiffness of the three-core cable sample is assessed through the four-point bending test at room temperature, as shown in Fig. 11. The setup comprises dual pairs of cable holder rings: inner rings affixed to the mobile frames and outer rings secured to a stable base. Ring sizes are adjusted to match the outer diameter of the tested cable. The mobility of the frames is restricted to vertical motions, ensuring controlled testing conditions. Displacement sensors are strategically placed on both the inner rings and the middle section of the cable to record associated displacements during the test. Simultaneously, the applied loading by the two inner rings is also recorded.

A 9-meter three-core cable sample underwent multiple pre-bending cycles to enhance contact between inner components, ensuring its mechanical behaviors are accurately represented in the subsequent test. Throughout the testing process, the applied loading induced bending and restoring in the cable, while maintaining a bending radius above

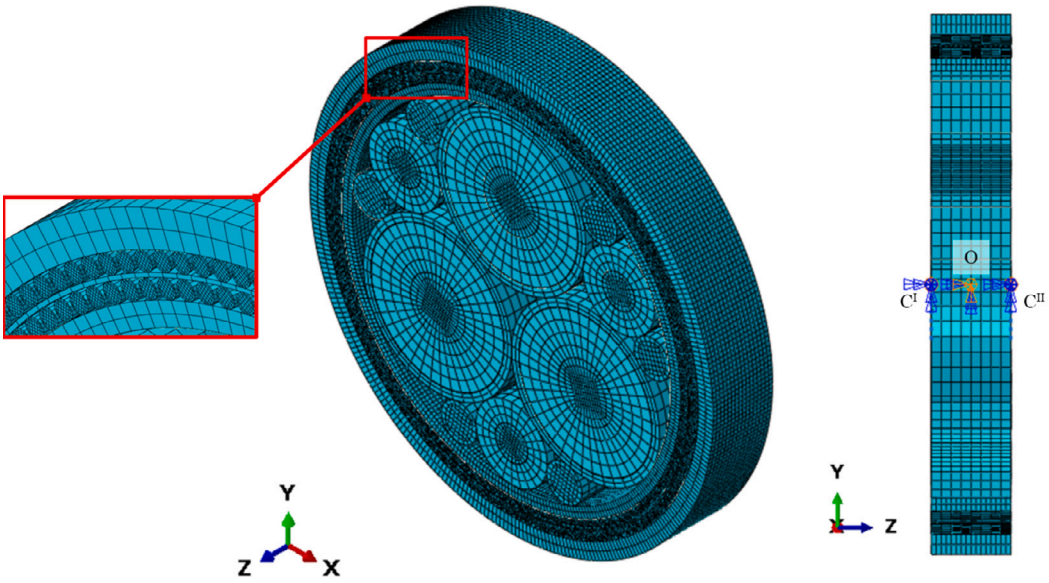

Fig. 8. Mesh of the whole RVE (left) and y-z plane view cut (right).

Fig. 9. Test samples of polymers (top) and photographs of material tests (base).

the sample's minimum requirement. Additionally, the loading was applied at a slow rate, deliberately chosen to minimize the impact of material strain-rate effects, thus enhancing the precision of the test results. The obtained bending stiffness from this three-core cable is used for model validation.

4. Model calibration and validation

Given that the RVE model integrates a dashpot technique to mitigate traction effects arising from the applied periodic boundary condition, we employ the test results from our prior collaborative work (Fang et al., 2023) on one-core cables for calibration. This calibration is crucial as it involves determining the dashpot-related damping coefficient in the RVE before validation. Subsequently, the RVE undergoes validation through testing with three-core cables. Additionally, we construct a full-scale FE model to compare with the RVE, aiming to assess its computational efficiency.

4.1. Calibration for dashpot coefficient

In a previous study (Fang et al., 2023), the four-point bending tests were conducted on one-core cable samples, as illustrated in Fig. 12. These samples, with a length of 600 mm, were uniformly bent to a curvature of 10^{-3} mm^{-1}. Corresponding one-core RVE model is constructed as shown in Fig. 13. The boundary conditions in this single-core model

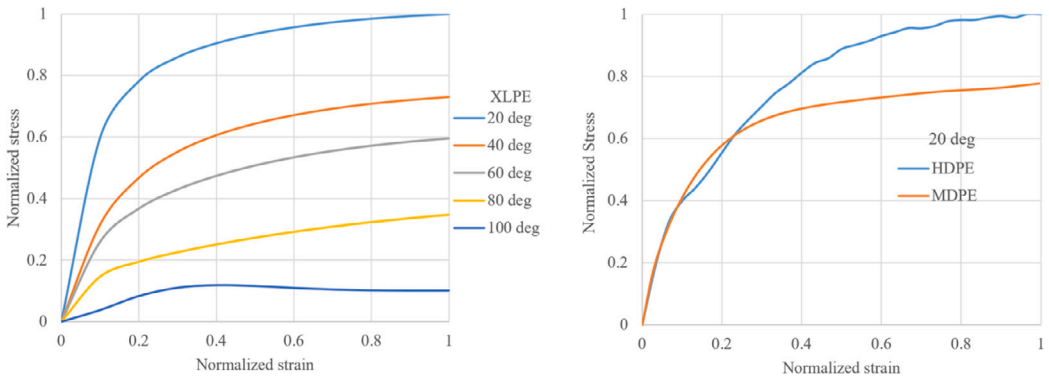

Fig. 10. Normalized strain vs. stress curves for XLPE under varying temperature (left) and for MDPE & HDPE at room temperature (right/20 °C).

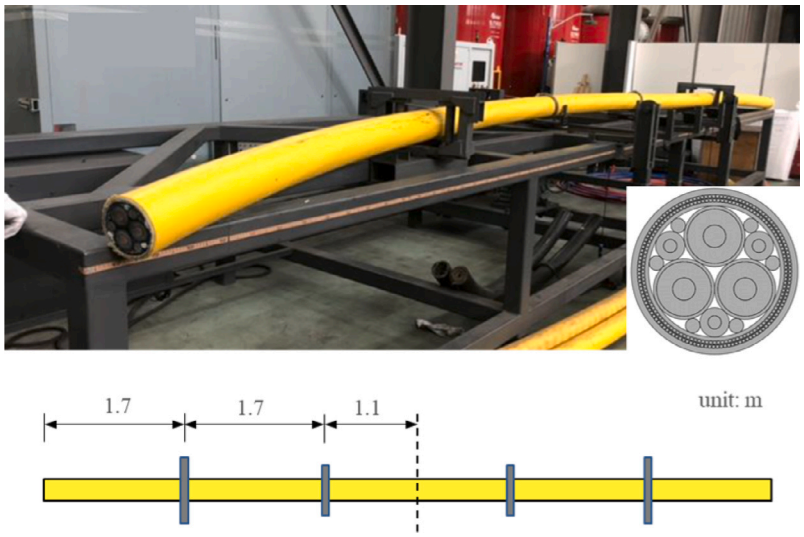

Fig. 11. Four-point bending test on three-core cable.

are identical to those in the three-core RVE. We varied dashpot damping coefficient, c_d, to investigate its impact on eliminating traction effects from the periodic condition. The bending stiffness curves from these cases are compared with test results to calibrate the dashpot coefficient.

The comparison of bending stiffness between tests and RVEs is illustrated in Fig. 14. It is evident that as the value of the dashpot coefficient increases, the stiffness in the RVE also rises. A notable match in overall bending behaviors with testing is achieved when this coefficient reaches a value of 1000. This suggests that when the dashpot coefficient is set to 1000, the traction force acting on armor wires due to the periodic boundary condition can be effectively offset. Consequently, the stick–slip behaviors of the wires are purely determined by their contact status.

4.2. Model validation and comparison

Following calibration, the RVE model for the three-core cable with a dashpot coefficient of 1000 is constructed for validation. To provide a comprehensive comparison, a 3D full-scale FE model is also constructed, as illustrated in Fig. 15, to assess the computing efficiency of this RVE. The length of this full-scale model is equal to the pitch of helical wires, ensuring a sufficiently long cable to eliminate end effects. The surface-based contact properties are set the same as in the RVE. The mesh size is well-adjusted to balance accuracy and efficiency given the three-core cable has an extremely complex structural configuration. However, the total elements count for this full FE model

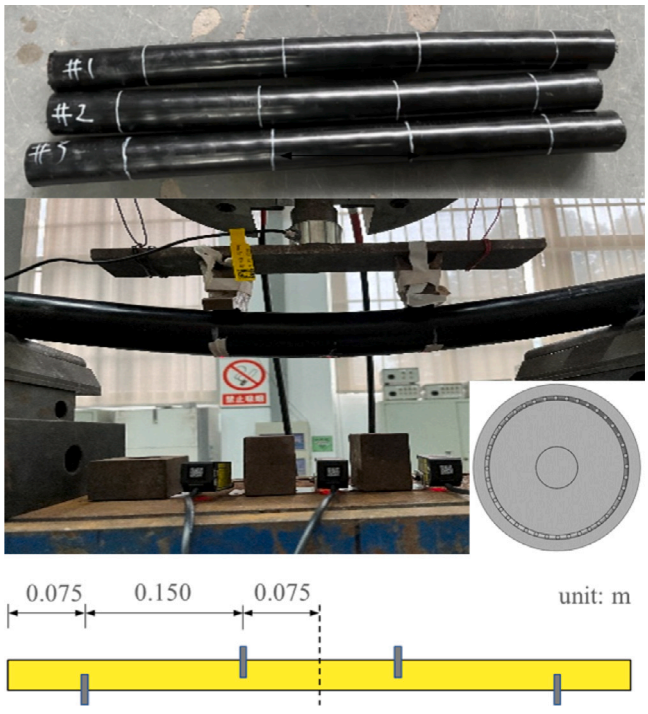

Fig. 12. Four-point bending test on one-core cables.

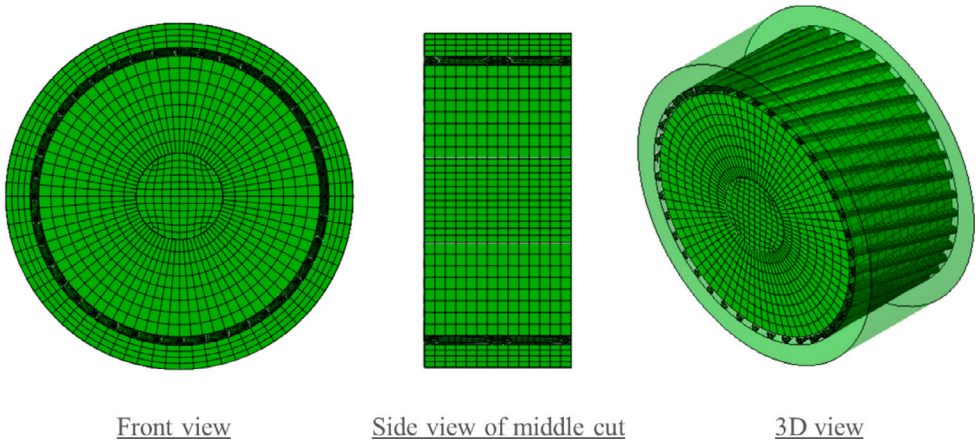

Fig. 13. RVE model for one-core cable in different views.

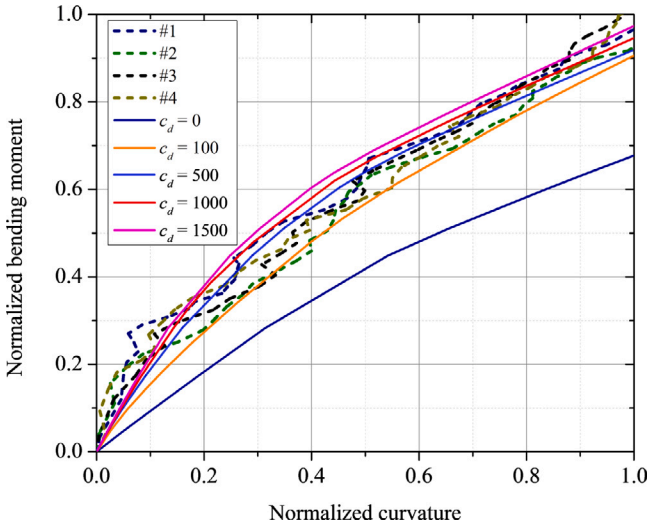

Fig. 14. Normalized curvature vs. bending moment obtained from tests and RVEs for one-core cable.

still approaches 3 million, resulting in a time-consuming computational process taking over one week on our HPC system with 32 cores.

Three reference points (RPs) are positioned on the left, middle, and right cross-sections of this full-scale FE model along its axial centerline, as depicted in Fig. 15. The RPs on the cable ends are allowed movement only within the y-z plane, coupling solely with nodes of non-metallic components. This setting aligns with the absence of restraints on the sample ends during testing, preventing over-constraining of the entire structure. Bending moments are applied to these two RPs to force the cable to bend symmetrically. The middle RP couples all the nodes on the middle section except the ones from helical armor wires, allowing stick–slip behaviors to take place. By fully fixing this middle RP, symmetric bending can thereby be imposed onto the cable.

The nonlinear stiffness curves from the RVE, 3D full model, and testing are plotted in Fig. 16. The outcome provided by the calibrated RVE model closely aligns with the other two, with an average difference of less than 10%. The test result exhibits a highly nonlinear hysteresis effect, clearly indicating transitions between stick and slip regimes. This characteristic is well-captured by both the full-scale FE model and RVE results. At small curvatures, internal friction hinders relative movement, leading to a relatively high tangent stiffness. Once the curvature surpasses a certain threshold, slippage rapidly occurs until the stiffness stabilizes.

The stress distribution over the cable's cross-section at the maximum bending curvature is compared between the full model and RVE, as shown in Fig. 17(a). Both the RVE and the full model exhibit a similar stress profile, except for the maximum stress. In the RVE, the maximum stress magnitude is nearly 2.5 times that of the full model, concentrated in the wire regions where the dashpots are applied to. This difference arises because the continuous helical wires in the RVE are reduced to segments, creating a misalignment between their centerline and the cable. Despite achieving periodicity, this misalignment causes bending moments to induce an additional 'traction effect' through the MPCs on those segments. The dashpot technique is thereby introduced in RVE to offset that traction effect, resulting in the wire withstanding additional loading and a much higher stress magnitude.

When the helical wires are removed, both the 3D full model and the RVE exhibit a similar stress distribution over the inner components as displayed in Fig. 17(b). In this scenario, the steel strands become the secondary components for internal mechanical protection. The maximum stress in the full model is around 90 MPa, whereas the RVE reaches only 55 MPa in the same component. This difference is owing to the fact that the helical wires and their associated dashpots in the RVE bear more external loads, diminishing the contribution from the inner components to the bending resistance. Consequently, the stress level of inner components in the RVE is lower than that in the full model.

Following test validation and full-scale FE model comparison, the RVE model is able to efficiently predict the bending stiffness of submarine power cables. As aforementioned, the full-scale FE model required over one week and 32 cores to complete the bending computation. In contrast, the RVE finishes the same task in less than six hours using only 8 cores. However, it is important to note that excessive stress induced by damping traction can lead to premature plasticity in wires, resulting in inaccurate stiffness predictions after reaching the material yielding point. Technical efforts to address this traction effect, such as surface-based contact damping or cohesion-damage techniques, have faced challenges with convergence. Among these attempts, dashpot damping has emerged as a viable solution, enabling the RVE to achieve both efficiency and accuracy.

5. Thermal effect on bending stiffness

As submarine power cables advance to accommodate high current capacities, they must endure a significant amount of heat during the energy transmission process. Thermal fluctuations may alter material properties, thereby influencing the safety and overall performance of the cable structure. While the cable industry acknowledges the thermal effect on cable bending, the lack of available models for investigation poses a challenge. In response, this study utilizes the validated

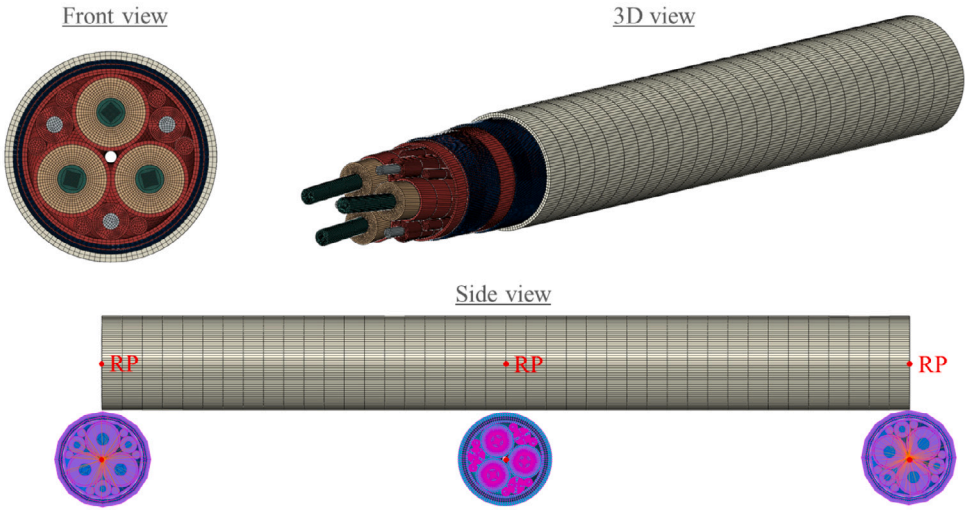

Fig. 15. 3D modeling of the full-scale three-core cable.

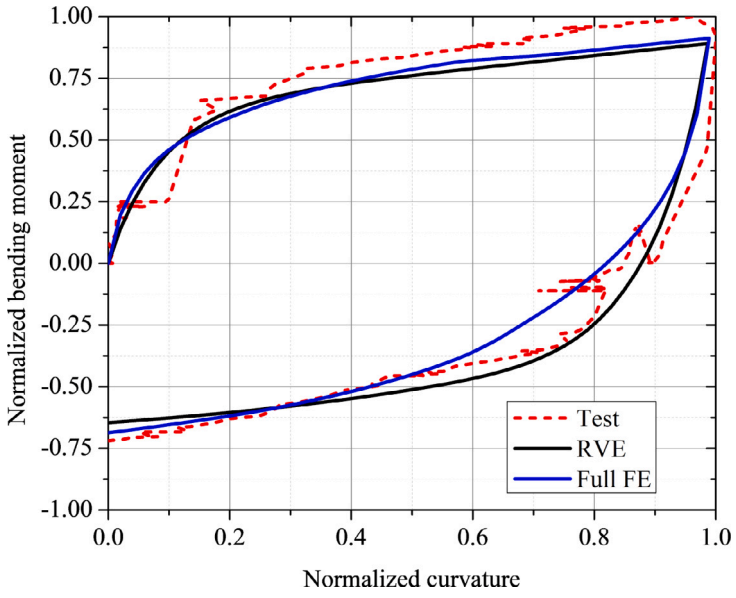

Fig. 16. Normalized curvature vs. bending moment obtained from tests, full model and RVEs for three-core cable.

Table 1
Thermal properties of materials (Hamdan, 2019; Yan et al., 2021; Bilgin et al., 2007).

Material	Thermal conductivity W (m K)$^{-1}$	Expansion coeff. 10^{-6} K^{-1}	Specific heat J (g K)$^{-1}$
Copper	320	19	0.385
Steel	18	12.3	0.48
XLPE	0.286	250	2.20
MDPE	0.39	165	1.90
HDPE	0.39	142	1.90

RVE model to explore the thermal impact on the bending stiffness of three-core cables.

Considering the insulation is designed to endure operational temperatures up to 90 °C, this study investigates bending behaviors across a temperature range from 20 to 90 °C. The conductors of the cable serve as heat sources, with an ambient temperature of 20 °C. Thermal properties of component materials are detailed in Table 1, referencing the works of Hamdan (2019), Yan et al. (2021), Bilgin et al. (2007), Hamdan et al. (2020).

This thermal–mechanical analysis comprises two steps. In the first step, the cable is preheated to generate the thermal field, considering three cases with conductor temperatures set at 20, 50, and 90 °C. This process is implemented using predefined field functions in Abaqus. In the second step, bending moments are applied to the cable to observe how the thermal condition influences its stiffness. The curvature vs. moment curve is graphically presented for each temperature scenario in Fig. 18, in which a significant reduction in bending stiffness is occurred with increasing conductor temperatures. At the maximum curvature, there is a 20% decrease in the cable bending stiffness when comparing the cases of 90 to 20 °C. This thermal-induced stiffness reduction aligns with findings observed in Maioli's cable bending test (Maioli, 2015).

Fig. 19 illustrates the contours of both thermal and mechanical fields at the maximum curvature. A comparison with the 20 °C temperature scenario reveals that in the cases of 50 and 90 °C, the internal metallic components – conductors and steel strands – progressively increase their contribution to the bending resistance. This phenomenon is linked to the thermal-induced material softening behavior of polymers, as depicted in Fig. 10, resulting in reduced contact pressure on helical

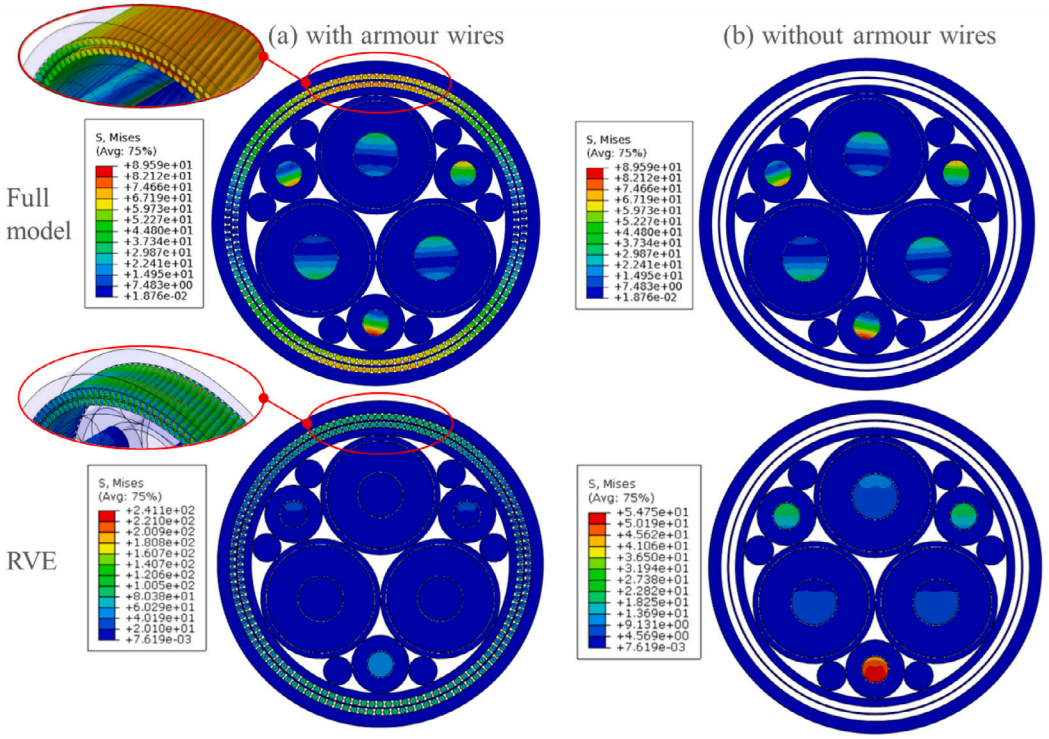

Fig. 17. Cross-sectional stress contour comparison with and without armoring wires at maximum curvature.

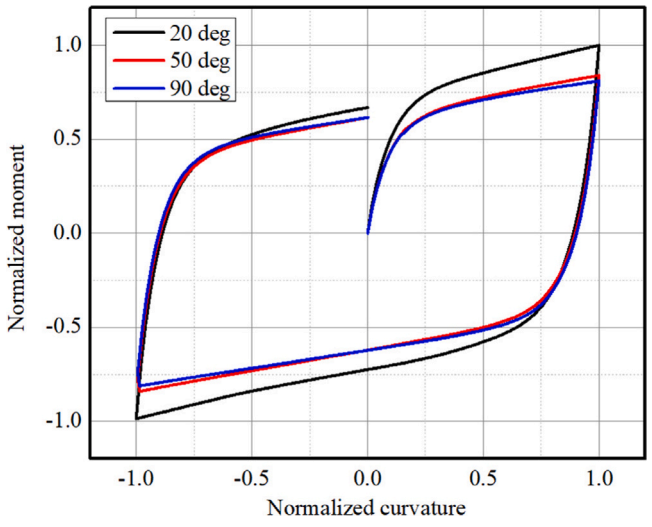

Fig. 18. Normalized curvature vs. bending moment from RVE for 20, 50, and 90 °C.

wires. With diminished wire friction, the cable gains flexibility and thereby induces greater stress levels on internal components.

Supporting evidence is presented in Fig. 20, illustrating the contact stress on the inner liner situated between the double armor layers. Key observations include a notably larger contact area at 20 °C compared to 50 and 90 °C. Simultaneously, the maximum contact stress at 20 °C is nearly double those of the latter temperatures. An intriguing discovery is that the maximum contact stress at 50 °C is slightly smaller than the one at 90 °C. This is caused by the interplay between the material softening behaviors and the thermal expansion effects, which influences the contact dynamics (Zhang et al., 2023a).

The study presented in this section, exploring the thermal impact on the bending stiffness of three-core cables, is still in the preliminary stage. The principal aim is to demonstrate the feasibility of the proposed RVE in integrating thermal effect into the analysis of cable bending behaviors. While this RVE reveals the susceptibility of cable bending stiffness to thermal variations, further research is essential to enhance its reliability and validate the findings. This may include detailed experimental investigations on the thermal-dependent mechanical behaviors of each component and their thermal–mechanical interactions, adjusting the periodic boundary conditions of RVEs accordingly. Additionally, when it comes to dynamic loading scenarios, the material strain-rate effect shall also be investigated to refine the RVE model.

6. Conclusions

To date, there is a lack of models in the public literature for analyzing the bending of submarine power cables, let alone involving thermal effect. While full-scale numerical simulations could be a choice, their high computational cost makes them less practical for design-stage bending analysis. In this study, a dashpot-enhanced RVE model is developed to predict the nonlinear bending behaviors of three-core submarine power cables. The RVE model employs the assumption of constant curvature and the periodic boundary conditions to efficiently minimize the cable length for modeling, simplifying the bending analysis process.

To validate the effectiveness of this RVE model, comprehensive tests and 3D full-scale FE models were carried out for thorough examination. Moreover, the validated RVE model was applied to investigate the thermal effects on the bending stiffness of the cable. The key findings and conclusions drawn from the entire study are as follows:

(1) The dashpot-enhanced RVE model developed in this study undergoes rigorous validation through mechanical bending tests. The predicted bending stiffness closely aligns with the result from the test, showcasing an average difference of less than 10%. This demonstrates that the utilization of periodic boundary conditions and dashpot technique enables accurate capturing of the stick–slip behavior in the bending of cables.

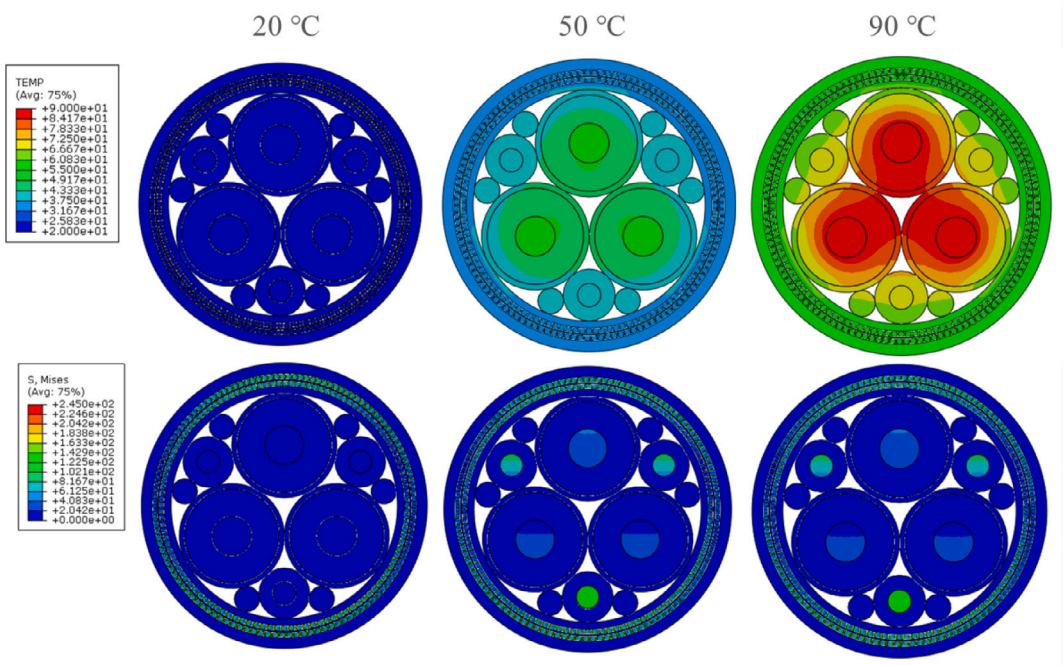

Fig. 19. Temperature and stress distribution over the cross section at maximum curvature.

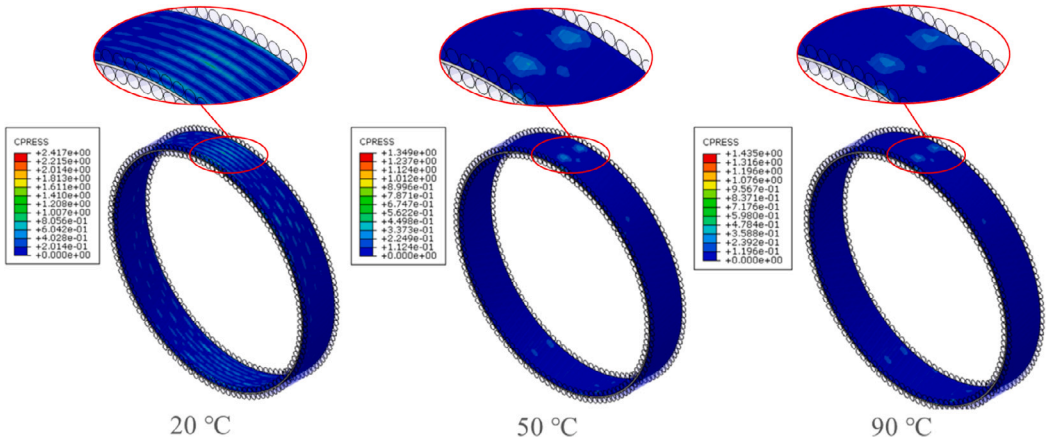

Fig. 20. Distribution of contact stress on inner liner at maximum curvature for each temperature case.

(2) The RVE model emerges as an efficient tool for mechanical analysis during the cable design stage. In our study, we evaluated the computing efficiency of this RVE by comparing it to a full-scale FE model for the same case. The full-scale numerical simulation required over one week to complete a single job, utilizing an HPC system with 32 cores. In contrast, the proposed RVE model significantly reduces computational time, completing the same task in less than six hours with only 8 cores.

(3) This RVE facilitates thermal–mechanical coupling analysis in the flexural design of cables. A preliminary investigation into the thermal effect on bending stiffness is conducted using the developed RVE, demonstrating its potential for multiphysics studies. The study reveals a decrease in bending stiffness with rising temperature. The main cause comes from the interplay between material softening and thermal expansion, influencing the contact dynamics between cable components.

This work demonstrates that the developed RVE model is able to be an effective tool for bending analysis during the cable design stage. The thermal–mechanical analysis presented with the RVE in this work represents an exploratory phase. With further studies and refinement, we anticipate that this RVE could evolve into a feasible approach to facilitate multiphysics analysis in cable design.

CRediT authorship contribution statement

Xiao Li: Writing – original draft, Validation, Methodology, Data curation, Conceptualization. **Zhuangjian Liu:** Supervision, Resources. **Xiaoli Jiang:** Writing – review & editing, Supervision, Resources. **Hans Hopman:** Writing – review & editing, Supervision, Resources.

Declaration of competing interest

We would like to state that the enclosed manuscript entitled "RVE Model Development for Bending Analysis of Three-Core Submarine Power Cables with Dashpot-Enhanced Periodic Boundary Conditions" has no conflict of interest. There are no financial and personal relationships with other people or organizations that can inappropriately

influence our work. I would like to declare on behalf of my co-authors that the work described was original research that has not been published previously, and not under consideration for publication elsewhere.

Acknowledgments

The authors gratefully acknowledge Prof. Yong Bai from Zhejiang University, China, and Mr. Pan Fang from Delft University of Technology, Netherlands, for their invaluable data support.

References

Amjadi, M., Fatemi, A., 2020. Tensile behavior of high-density polyethylene including the effects of processing technique, thickness, temperature, and strain rate. Polymers 12 (9), 1857.

Axelsson, G., Skjerve, H., 2014. Flexible riser carcass collapse analyses - sensitivity on radial gaps and bending. In: Proceedings of the 33rd International Conference on Ocean, Offshore and Arctic Engineering. American Society of Mechanical Engineers, San Francisco, California, USA, OMAE2014-23922.

Bilgin, Ö., Stewart, H., O'Rourke, T., 2007. Thermal and mechanical properties of polyethylene pipes. J. Mater. Civ. Eng. 19, 1043–1052.

Caleyron, F., Guiton, M., Leroy, J.M., Perdrizet, T., Charliac, D., Estrier, P., Paumier, L., 2014. A multi-purpose finite element model for flexible risers studies. In: Proceedings of the 33rd International Conference on Ocean, Offshore and Arctic Engineering. American Society of Mechanical Engineers, San Francisco, California, USA, OMAE2014-23250.

Chang, H.C., Chen, B.F., 2019. Mechanical behavior of submarine cable under coupled tension, torsion and compressive loads. Ocean Eng. 189, 106272.

COREWIND, 2020. D3.1 review of the state of the art of dynamic cable system design. INNOSEA/ JDR/ RAMBOLL/ IREC/ COBRA/ UL DEWI/ WINDEUROPE.

Corre, V.L., Probyn, I., 2009. Validation of a 3-dimensional finite element analysis model of a deep water steel tube umbilical in combined tension and cyclic bending. In: Proceedings of the 28th International Conference on Ocean, Offshore and Arctic Engineering. American Society of Mechanical Engineers, Honolulu, Hawaii, USA, OMAE2009-79168.

DeCastro, M., Salvador, S., Gómez-Gesteire, M., Garvalho, D., Sanz-Larruga, F.J., Gimeno, L., 2019. Europe, China and the United States: Three different approaches to the development of offshore wind energy. Renew. Sustain. Energy Rev. 109, 55–70.

Euler, L., Formulae generales pro translatione quacunque corporum rigidorum (general formulas for the translation of arbitrary rigid bodies). Novi Comment Acad. Sci. Petropolitanae 20 (1776), 189–207.

Fang, P., Li, X., Jiang, X., Hopman, H., Bai, Y., 2023. Bending study of submarine power cables based on a repeated unit cell model. Eng. Struct. 293, 116606.

Feret, J.J., Bournazel, C.L., 1987. Calculation of stresses and slip in structural layers of unbonded flexible pipes. J. Offshore Mech. Arctic Eng. 109 (3), 263–269.

Gay Neto, A., Martins, C.A., 2014. Flexible pipes: influence of the pressure armor in the wet collapse resistance. J. Offshore Mech. Arctic Eng. 136 (3), 031401.

Guttner, W.C., Santos, C.C.P., Pesce, C.P., 2017. A finite element method assessment of a steel tube umbilical (STU) cable subjected to crushing load: comparison between two and three-dimensional approaches. Mar. Struct. 53, 52–67.

Hall, M., Sirnivas, S., Yu, Y., 2021. Implementation and verification of cable bending stiffness in MoorDyn. In: Proceedings of the AMSE 2021 3rd international offshore wind technical conference. American Society of Mechanical Engineers, Virtual, Online, IOWTC2021-3565.

Hamdan, M.A., 2019. Analysis of Thermo-Mechanical Stresses in Joints and Cables (Ph.D. dissertation). Univ Southampton.

Hamdan, M.A., Pilgrim, J.A., Lewin, P.L., 2020. Analysis of thermo-mechanical stress in three core submarine power cables. IEEE Trans. Dielectr. Electr. Insul. 27 (4), 1288–1296.

Hedlund, J., 2015. Modelling of viscoelastic dynamic bending stiffness for VIV analysis of submarine cables. In: Proceedings of the 9th International Conference on Insulated Power Cables. Versailles, France.

Jordal, L., Slora, R., Vermeer, E., Komperød, 2017. A novel bending stiffness rig for identification of sub-sea cables' and umbilicals' sensitivity to temperature under sinusoidal curvature oscillations. In: Proceedings of the 27th International Ocean and Polar Engineering Conference. ISOPE 2017. San Francisco, California, USA.

Kebadze, E., 2000. Theoretical Modelling of Unbonded Flexible Pipe Cross-Sections (MSc dissertation). South Bank Univ.

Kinsella, M.E., Lilly, B., Gardner, B.E., Jacobs, N.J., 2005. Experimental determination of friction coefficients between thermoplastics and rapid tooled injection mold materials. Rapid Prototyp. J. 11 (3), 167–173.

Kirchhoff, G., 1859. Ueber das Gleichgewicht und die Bewegung eines unendlich dünnen elastischen stabes (On the balance and movement of an infinitely thin elastic rod) J. Reine Angew. Math. 56, 285–313.

Komperød, M., Juvik, J.I., Evenset, G., Slora, R., Jordal, L., 2017. Large-scale tests for identifying the nonlinear, temperature-sensitive, and frequency-sensitive bending stiffness of the NORDLINK cable. In: Proceedings of the 36th International Conference on Ocean, Offshore and Arctic Engineering. American Society of Mechanical Engineers, Trondheim, Norway, OMAE2017-61103.

Kraincanic, I., Kebadze, E., 2001. Slip initiation and progression in helical armoring layers of unbounded flexible pipes and its effect on pipe bending behavior. J. Strain Anal. Eng. Des. 36 (3), 265–275.

Lanteigne, J., 1986. Theoretical estimation of the response of helically armored cables to tension, torsion, and bending. ASME J. Appl. Mech. 52 (2), 423–432.

Leroy, J.M., Estrier, P., 2001. Calculation of stresses and slips in helical layers of dynamically bent flexible pipes. Oil Gas Sci. Technol. 56 (6), 545–554.

Li, X., Jiang, X., Hans, H., 2021a. Development of an analytical model for predicting the wet collapse pressure of curved flexible risers. Ocean Eng. 232, 109132.

Li, X., Jiang, X., Hopman, H., 2021b. Curvature effect on wet collapse behaviors of flexible risers subjected to hydro-static pressure. Ships Offshore Struct. 232, 109132.

Li, X., Vaz, M.A., Custódio, A.B., 2019. Analytical model for tensile armors lateral deflections and buckling in flexible pipes. Mar. Struct. 64, 211–228.

Lu, Q., Chen, J., Yang, Z., Yin, Y., Yue, Q., 2017a. Numerical and experimental analysis of umbilical cables under tension. Adv. Compos. 26 (2), 56–62.

Lu, Q., Yang, Z., Yan, J., Lu, H., Chen, J., Yue, Q., 2017b. A finite element model for prediction of the bending stress of umbilicals. J. Offshore Mech. Arct. Eng. 39, 061302-1.

Lukassen, T.V., Gunnarsson, E., Krenk, S., Glejbøl, K., Lyckegaard, A., Berggreen, C., 2019. Tension-bending analysis of flexible pipe by a repeated unit cell finite element model. Mar. Struct. 64, 401–420.

Maioli, P., 2015. Bending stiffness of submarine cables. In: Proceedings of the 9th International Conference on Insulated Power Cables. Versailles, France.

Matine, A., Drissi-Habti, M., 2019. On-coupling mechanical, electrical and thermal behavior of submarine power phases. Energies 12 (6), 1–11.

Ménard, F., Cartraud, P., 2021. Solid and 3D beam finite element models for the nonlinear elastic analysis of helical strands within a computational homogenization framework. Comput. Struct. 257, 106675.

Ménard, F., Cartraud, P., 2023. A computationally efficient finite element model for the analysis fo the non-linear bending behavior of a dynamical submarine power cable. Mar. Struct. 91, 103465.

Mullins, J., Morin, D., Tyrberg, A., Sonesson, C., Ekh, J., 2015. Bitumen shear mechanics in a dynamic subsea electrical cable. In: Proceedings of the 34th International Conference on Ocean, Offshore and Arctic Engineering. American Society of Mechanical Engineers, St. John's, Newfoundland, Canada, OMAE2015-41110.

Out, J.M.M., Morgen, B.J., 1997. Slippage of helical reinforcing on a bent cylinder. Eng. Struct. 19 (6), 507–515.

Ramos, R., Pesce, C.P., Martins, C.A., 2003. A new analytical expression to estimate the bending stiffness of flexible riser. In: Proceedings of the 22nd International Conference on Offshore Mechanics and Arctic Engineering. Cancun, Mexico.

Resner, L., Paszkiewicz, S., 2021. Radial water barrier in submarine cables, current solutions and innovative development directions. Energies 14 (10), 2761.

Sævik, S., 2011. Theoretical and experimental studies of stresses in flexible pipes. Comput. Struct. 89, 2273–2291.

Sævik, S., Ye, N., 2016. Aspects of Design and Analysis of Offshore Pipelines and Flexibles. Southwest Jiaotong Univ Press, Chengdu, China.

Simulia, 2022. ABAQUS user's manual, version 2022.

Skeie, G., Sødahl, N., Steinkjer, O., 2012. Efficient fatigue analysis of helix elements in umbilicals and flexible risers: theory and applications. J. Appl. M 1–22.

Smith, D.M., Cunningham, L.S., Chen, L., 2023. Efficient finite element modelling of helical strand cables utilising periodicity. Int. J. Mech. 108792.

Tang, M., Li, S., Zhang, H., Bian, X., Zhao, X., 2022. Monitoring the slip of helical wires in flexible riser under combined tension and bending. Ocean Eng. 256, 111512.

Tjahjanto, D.D., Tyrberg, A., Mullins, J., 2017. Bending mechanics of cable cores and fillers in a dynamic submarine cable. In: Proceedings of the 36th International Conference on Ocean, Offshore and Arctic Engineering. American Society of Mechanical Engineers, Trondheim, Norway, OMAE2017-62553.

Tyrberg, A., Tjahjanto, D., Hedlund, J., 2019. Bending stiffness of submarine cables - an experimental and numerical investigation. In: Proceedings of the 10th International Conference on Insulated Power Cables. Versailles, France.

Wang, W., Yan, X., Li, S., Zhang, L., Ouyang, J., Ni, X., 2021. Failure of submarine cables used in high-voltage power transmission: characteristics, mechanisms, key issues and prospects. IET Gener. Transm. Distrib. 15, 1387–1402.

Witz, J., Tan, Z., 1992. On the flexural structural behavior of flexible pipes, umbilicals and marine cables. Mar. Struct. 5 (2–3), 1992.

Yan, J., Su, Q., Bu, Y., Lu, Q., Yang, Z., 2022. Study on the nonlinear tension-torsion coupled stiffness of the high-current composite umbilical considering the thermal effect. China Ocean Eng. 36 (4), 588–600.

Yan, J., Su, Q., Bu, Y., Yang, Z., Lu, Q., Yue, Q., 2021. Electro-thermal-mechanical coupled analysis on two high-current composite umbilical cable cross sections. J. Offshore Mech. Arct. Eng. 143, 061802-1.

Yang, Z., Su, Q., Yan, J., Wu, S., Mao, Y., Lu, Q., Wang, H., 2021. Study on the nonlinear mechanical behaviours of an umbilical under combined loads of tension and torsion. Ocean Eng. 238, 109742.

Yun, R.H., Jang, B.S., Kim, J.D., 2020. Improvement of the bending behavior of a flexible riser: part I - nonlinear bending behavior considering the shear deformation of polymer layers. Appl. Ocean Res. 101, 102204.

Zhang, G., Chen, X., Yang, D., Wang, L., He, X., Zhang, Z., 2023a. Multi-physics coupling simulation technique for phase stable cables. Electronics 12 (1602), 1–11.

Zhang, X., Wang, S., Ma, W., Su, L., Yang, Y., 2023b. Study on the influence of bending curvature on bending characteristics of unbonded flexible pipes. Ocean Eng. 281, 114730.